



OPEN

SUBJECT AREAS:

MECHANICAL AND
STRUCTURAL PROPERTIES
AND DEVICES

SYNTHESIS OF GRAPHENE

ELECTRONIC MATERIALS

ELECTRONIC DEVICES

Spontaneous Reduction and Assembly of Graphene oxide into Three-Dimensional Graphene Network on Arbitrary Conductive Substrates

Chuangang Hu^{1*}, Xiangquan Zhai^{1*}, Lili Liu¹, Yang Zhao¹, Lan Jiang² & Liangti Qu¹Received
25 April 2013Accepted
10 June 2013Published
25 June 2013Correspondence and
requests for materials
should be addressed to
L.T.Q. (lqu@bit.edu.cn)* These authors
contributed equally to
this work.

¹Key Laboratory of Cluster Science, Ministry of Education, School of Chemistry, Beijing Institute of Technology, Beijing 100081, China, ²Laser Micro-/Nano-Fabrication Laboratory, School of Mechanical Engineering, Beijing Institute of Technology, Beijing 100081, China.

Chemical reduction of graphene oxide (GO) is the main route to produce the mass graphene-based materials with tailored surface chemistry and functions. However, the toxic reducing circumstances, multiple steps, and even incomplete removal of the oxygen-containing groups were involved, and the produced graphenes existed usually as the assembly-absent precipitates. Herein, a substrate-assisted reduction and assembly of GO (SARA-GO) method was developed for spontaneous formation of 3D graphene network on arbitrary conductive substrates including active and inert metals, semiconducting Si, nonmetallic carbon, and even indium-tin oxide glass without any additional reducing agents. The SARA-GO process offers a facile, efficient approach for constructing unique graphene assemblies such as microtubes, multi-channel networks, micropatterns, and allows the fabrication of high-performance binder-free rechargeable lithium-ion batteries. The versatile SARD-GO method significantly improves the processability of graphenes, which could thus benefit many important applications in sensors and energy-related devices.

Graphene, an atomic-thick layer of carbon atoms with unique properties such as high electrical conductivity, large surface area, good chemical, environmental and mechanical stability, has drawn extensive attention from both the experimental and theoretical communities due to its promising applications in energy, environment, biology, and electronics^{1–6}.

For preparation of graphenes, chemical reduction of graphene oxide (GO) is one of the most important routes owing to its feasibility for mass production of graphene-based materials with tailored surface chemistry and functions⁷. However, chemical treatment of GO was usually carried out in reducing circumstances such as hydrazine (N₂H₄)⁸, H₂/Ar with alcohol under high temperatures⁹, strong alkaline sodium/potassium hydroxide^{10,11}, sodium borohydride/sulfuric acid¹², hydriodic acid¹³, sodium-ammonia solution¹⁴. Besides that the reduction reactions are often involved in the toxicity of the reducing agents, multiple steps, long reaction time, and even incomplete removal of the oxygen-containing groups¹⁵, the produced graphenes are usually collected as random precipitates or agglomeration lacking of well-confined organization such as three-dimensional (3D) graphene assemblies^{16–19}, which largely limit their applications in energy-related devices.

The recent findings that GO can be directly reduced by active metals (e.g., Al, Fe, Cu)^{20–22} open the new possibility for controlled assembly of graphenes on conductive substrates. Herein, we demonstrate a powerful, facile but efficient substrate-assisted reduction and assembly of GO (SARA-GO) (Figure 1). The spontaneous reduction of GO and its well-organized assembly into 3D network on arbitrary conductive surfaces such as the active metals of Zn, Fe, and Cu, inert metals of Ag, Pt, and Au, semiconducting Si wafer, nonmetallic carbon-based film, and even indium-tin oxide (ITO) glass are achieved readily without any additional reducing agents. As we shall see later, the versatile SARD-GO method offers an efficient approach for constructing a variety of unique graphene assemblies such as microtubes, four-way pipes, spiral tubes, multi-channel networks, and micropatterns, and allowing the fabrication of high-performance binder-free rechargeable lithium-ion batteries (LIBs) by spontaneously deposition of 3D graphene network on Cu foil as anode. The SARD-GO method significantly improves the versatile process of graphenes, which could thus benefit many important applications of graphenes in sensors and energy-related devices.

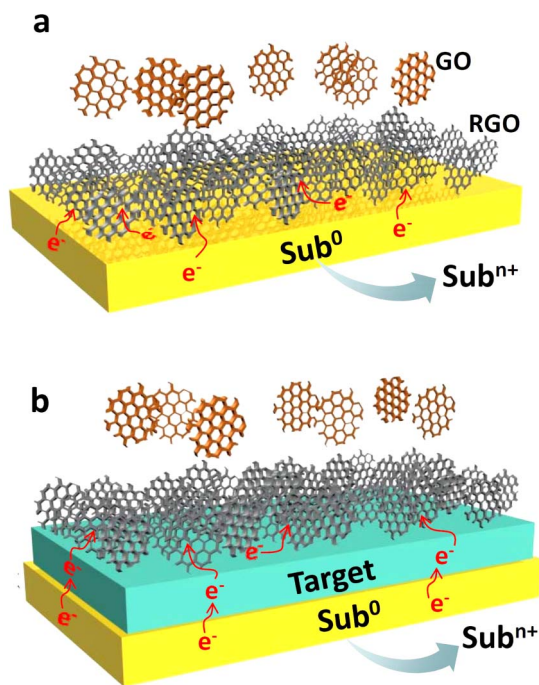


Figure 1 | SARD-GO process. Schemes of the SARD-GO process on (a) active metal substrate and (b) on the arbitrary conductive target supported by active metal. The active metal substrates (Sub^0) are oxidized to Sub^{n+} ions with electron (e^-) loss, while the GO is reduced by electron reception. The electron transport through the target to the GO allows the 3D assembly of RGO on it.

Results

SARA-GO on active metal surface. As one example, the Cu foil has been standing in the aqueous 1 mg/mL GO suspension with a pH = 4.0 for several hours without any additives, a black layer of reduced GO (RGO) covers its whole surface (Fig. 2a and Supplementary Fig. S1), which is composed of the 3D network of RGO sheets (Fig. 2b and Supplementary Fig. S2). The amount of deposited RGO on Cu foil can be modulated conveniently by the reaction time (Supplementary Fig. S3).

TEM investigation reveals that the as-prepared RGO sheets are decorated with nanoparticles (Fig. 2c), which are easily removed after washing with aqueous HCl solution (Fig. 2d, and Supplementary Fig. S4). Electron diffraction pattern of the RGO sheets presents clear diffraction spots without halation (Fig. 2d, inset), implying the highly crystalline graphene structure.

X-ray diffraction (XRD) further confirms that the representative peak of GO ($2\theta = \text{ca. } 11^\circ$, the bottom curve in Fig. 2e) has completely disappeared in the as-prepared RGO samples, accompanied with a new broad peak centered at around 24° and a series of sharp peaks (the middle curve in Fig. 2e). The peaks at $2\theta = \text{ca. } 40^\circ, 47^\circ, 68^\circ, 82^\circ$, and 86° correspond to the (111), (200), (220), (311) and (222) planes of face-centered cubic (fcc) structure of Cu_2O (JCPDS ICDD card NO. 01-1194). After washed with aqueous HCl solution, the RGO presents a dominant peak centered at $2\theta = \text{ca. } 24^\circ$ (the upper curve in Fig. 2e), corresponding to the (002) plane of stacked graphene sheets with an interlayer spacing of about 0.37 nm. It is larger than the d -spacing (0.336 nm) of graphite, suggesting the incompact stacking of as-produced graphenes in the sample.

The chemical structure of the RGO deposited on Cu foil was also studied by Raman and X-ray photoelectron spectroscopy (XPS). Raman spectrum indicates that GO sheets were reduced and their conjugated structures were partly restored (Supplementary Fig. S5). XPS analysis shows that the intensity of O peak for RGO has

decreased drastically in comparison with GO (Fig. 2f). A Cu peak appears on the as-prepared RGO (the middle curve in Fig. 2f) and on the residues in the GO suspension (Supplementary Fig. S6), suggesting the Cu has been involved in the reduction reaction of GO. The Cu related peaks vanished in the RGO sample with aqueous HCl treatment (Fig. 2f, the upper curve) in consistent with the XRD observation. Fig. 2g shows the high resolution Cu2p spectrum, which reveals that Cu exists in an oxidized form with two peaks at around 932.2 and 951.9 eV assigned to Cu 2p_{3/2} and Cu 2p_{1/2} of Cu^+ , respectively^{23,24}. The XPS also indicates the presence of Cu^{2+} , suggesting that the surfaces of the Cu_2O nanoparticles were partially oxidized to CuO. The results are consistent with other observations of copper oxidation at the nanoscale^{25–27}. Combined with the fact that no diffractions from CuO were detected in XRD pattern (the middle curve Fig. 2e), it can be concluded that only a small amount of Cu_2O was oxidized and/or the formed CuO might be amorphous.

High resolution C1s peak of the final RGO proves that oxygen-containing groups have been removed significantly. The C1s spectrum of the original GO (Fig. 2h) reveals four types of carbon bonds: C=C/C–C (~ 284.8 eV), C–O (hydroxyl and epoxy, ~ 286.6 eV), C=O (carbonyl, ~ 287.5 eV) and O–C=O (carboxyl, ~ 288.7 eV)²⁵. For the RGO formed on Cu foil, however, the majority of oxygen functional groups have been removed and the C–C bonds become dominant (Fig. 2h). The C/O atomic ratio of RGO is ca. 9.1 (Table S1), which, although not the best, is much higher than that of RGO synthesized by other typical reduction process (Table S2).

Through the extensive investigation mentioned above, we conclude that, based on the SARA-GO in Fig. 1a, GO has been spontaneously reduced to graphene (also called RGO in this work) in a 3D network form, while the Cu substrate is oxidized into the Cu oxide. Other active metals such as Al, Zn, Fe, Co also play well for direct formation the 3D graphene network on their foils (Fig. 2i–l and Supplementary Fig. S7–S16).

SARA-GO on inert metal surface. Although the spontaneous reduction of GO induced by active metals is impressive as demonstrated in current work and others^{22–24}, it is not yet applicable to the inert metals such as Ag, Pt and Au (Supplementary Fig. S16), not to mention the nonmetallic conductive substrates. The reduction of GO and the oxidation of metal substrates are associated with the electron harvest of GO and the electron loss of metal (Fig. 1a), which provides the opportunity to reduce GO onto arbitrary conductive surfaces *via* SARA-GO process in Fig. 1b. This concept is inspired by the substrate-enhanced electroless deposition (SEED) we developed previously²⁶. As schematically shown in Fig. 1b, by simply supporting the inert metals or other conductive surfaces (Target) with an active metal substrate (Sub^0), GO could be reduced and deposited on the Target surface via a process analogous to the galvanic displacement reaction²⁶. The inert conductive substrate acts as a “cathode” for GO reduction and deposition of RGO from its suspension, while the active metal foil serves as an “anode” where Sub^0 is oxidized into Sub^{n+} . Therefore, the SARA-GO process should allow the assembly of RGO on any conducting substrate as long as a proper base substrate is defined.

To demonstrate this concept, we supported the inert Au sheet (purity: 99.9%) with the Cu foil (Au/Cu) and exposed them to the aqueous GO suspension. As can be seen in Fig. 3b, the Au surface is covered with graphene network just like the porous structure on Cu foil (Fig. 2b), while the Au sheet without Cu support remains clear regardless of the reaction time (Fig. 3a). These results confirm the effective deposition of RGO network on inert metal surface via the SARA-GO.

TEM investigation reveals the transparent RGO sheet with clear electron diffraction spots (Fig. 3c and inset) characteristic of the highly crystalline graphene structure. XRD further confirms that the representative peak of GO ($2\theta \approx 11^\circ$) has completely disappeared

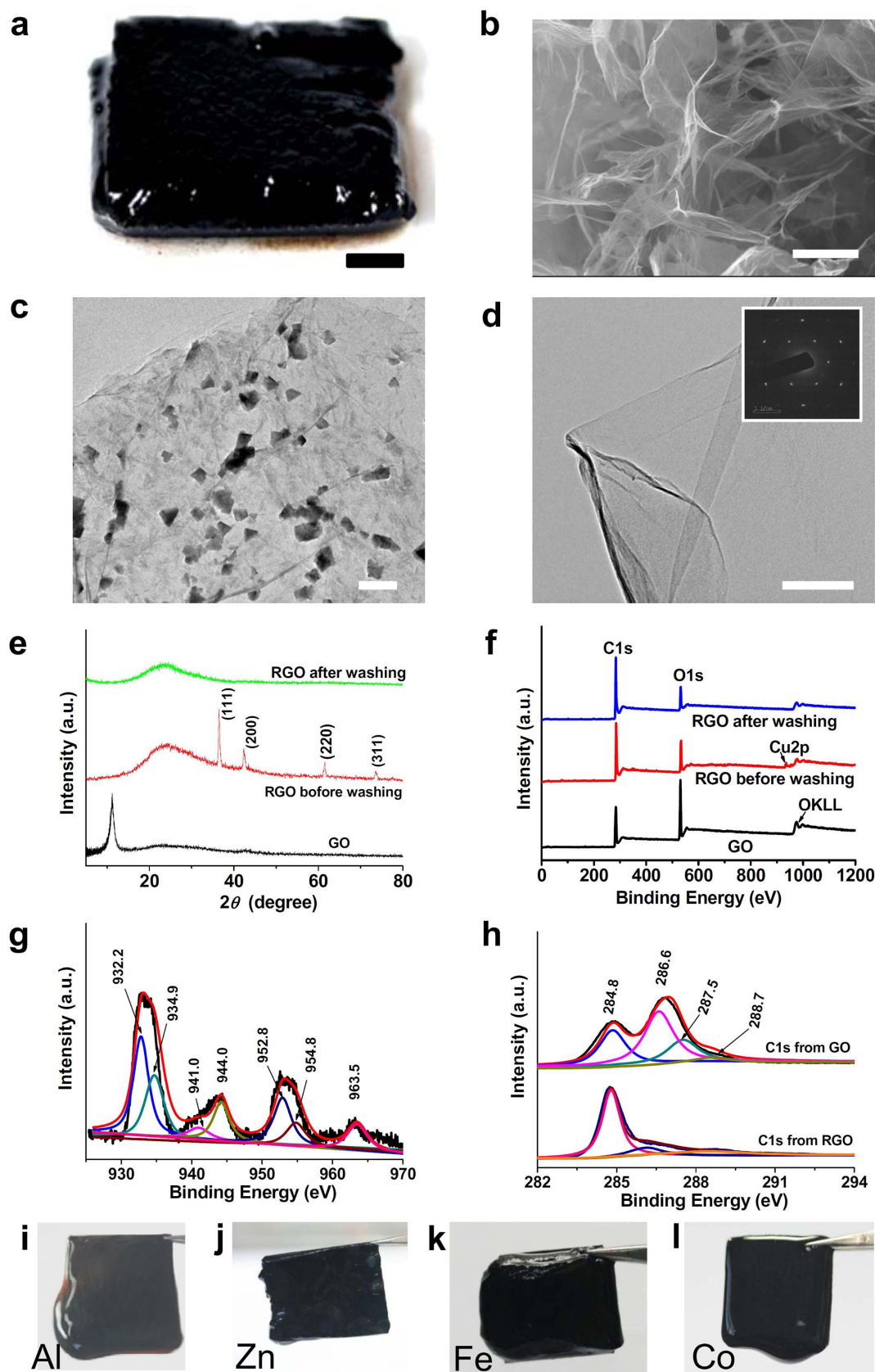


Figure 2 | SARA-GO on active metal surface. (a) A photograph of the as-deposited 3D RGO on Cu foil. (b) SEM image of the freeze-dried sample in (a). (c and d) TEM images of RGO on Cu foil before and after treatment with aqueous HCl solution, respectively. The inset in (d) is the corresponding electron diffraction pattern. (e and f) XRD patterns and XPS spectra of initial GO, as-deposited RGO on Cu before and after washing with aqueous HCl solution, respectively. (g) High-resolution of Cu 2p peak of RGO as shown in (c) before washing with aqueous HCl solution, and (h) C1s peak comparison of GO with RGO after washing with aqueous HCl solution. (i–l) Photographs of Al, Zn, Fe and Co foils (ca. $2 \times 3 \text{ cm}^2$) as-deposited with RGO. Scale bars: (a), 1 cm; (b), 10 μm ; (c), 200 nm; (d), 100 nm.

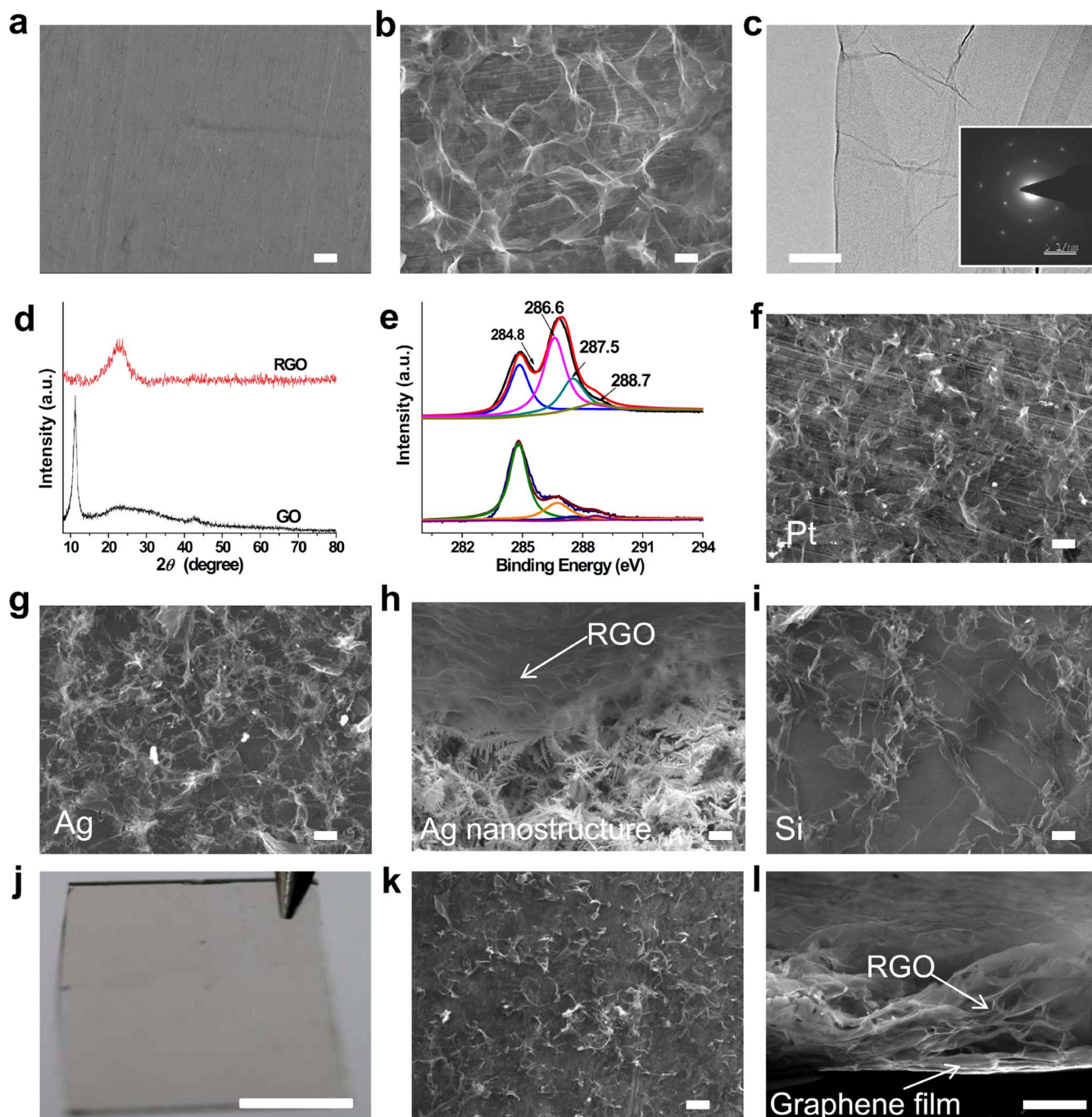


Figure 3 | SARA-GO on inert metal surfaces and nonmetallic surfaces. (a and b) SEM images of Au surfaces without and with Cu support after exposure to 1 mg/mL GO solution and lyophilization, respectively. (c) TEM image and electron diffraction pattern of RGO produced on Au surface supported by Cu by SARA-GO. (d and e) XRD patterns and high-resolution of C 1s peaks of RGO produced on Au surface supported by Cu in comparison with initial GO, respectively. (f–h) SEM images of RGO produced on Pt, Ag and Ag nanostructure surfaces supported with Cu, respectively. (i) SEM image of RGO produced on semiconducting Si supported with Cu. (j and k) Photograph and SEM image of ITO (ca. $2 \times 3 \text{ cm}^2$) with RGO on it by SARA-GO, respectively. (l) SEM image of RGO produced on graphene film supported by Cu foil. Scale bars: (a, b, f, g, h, i), and (k), 10 μm ; (c), 100 nm; (j), 1 cm; (l), 100 μm .

in the RGO samples, accompanied with a new broad peak centered at around 23° for loosely stacked graphenes (Fig. 3d). Accordingly, the C 1s XPS spectra of GO and RGO (Fig. 3e) reflect that most of the oxygenated functional groups of GO have been removed. The C/O ratio for the RGO on Au surface is 7.8, in consistent with that of RGO mentioned above (Fig. 2h). These characterizations demonstrate the deposited RGO network on Au surface has a feature of high-quality graphene similar to that on Cu, indicating the feasibility of SARA-GO.

Apart from the Au, the SARA-GO process also works well on such inert metals as Pt and Ag when their sheets were supported by Cu layers (Fig. 3f&g, and Supplementary Fig. S17). Similarly, RGO network can also be deposited on the Cu covered inert metals, such as Pt, Ag and Au (Supplementary Fig. S18).

To further demonstrate the effectiveness of SARA-GO process on the nanostructures of inert metals, we have put the Au, Ag, and Pt nanostructures with different sizes and shapes on Cu foil into the aqueous GO suspension (Supplementary Fig. S19). As expected, they



behavior as the good substrates to reduce the GO and assemble 3D RGO network on them (Supplementary Fig. S20–S22), indicating the morphology-independent feature of the practicable SARA-GO. Fig. 3h shows the deposited RGO network on Ag nanoleaves.

SARA-GO on nonmetallic surface. More importantly, the SARA-GO process allows the RGO spontaneously deposited on any conductive surfaces such as semiconducting Si (Fig. 3i and Supplementary Fig. S23&24), ITO glass (Fig. 3j&k and Supplementary Fig. S25), carbon (Fig. S26) and graphene films (Fig. 3l and Supplementary Fig. S27&28), indicating the versatile SARA-GO method is universal for formation of graphene network on conductive surfaces for various applications. Specially, the RGO network formed on ITO surface can have no obvious influence on the transparency with a proper reaction time (Fig. 3j&k and Supplementary Fig. S25).

Fabrication of graphene microtubes, four-way pipe, multi-channel network and graphene micropatterns via SARA-GO process. The SARA-GO process allowing the spontaneous reduction of GO on various conductive surfaces offers a facile but efficient method for construction of unique graphene assemblies of practical importance. As exemplified in Fig. 4a&b, the reduction of GO along a Cu wire will lead to the formation of graphene microtube (μ GT)^{27,28}. The Cu wire will act as the support for aggregation of RGO network, and meters of μ GTs with a diameter depending on the used Cu wire are collected after Cu etching in aqueous FeCl_3/HCl solution (Fig. 4b, Supplementary Fig. S29–S31). Further, specifically defined configurations such as spiral tubes (Fig. S32), four-way pipe (Fig. 4c, Supplementary Fig. S33), and multi-channel network of graphenes (Fig. 4f, Supplementary Fig. S34) with tunable length and diameter in large scale can be done readily.

Fig. 4c displays the as-prepared four-way pipe, and the inserts in Fig. 4c are the SEM images for the four nozzles, indicating the characteristics of hollow interior as the schematic diagram in Fig. 4d. Similarly, Cu mesh (Fig. 4e), as well as the Fe mesh (Supplementary Fig. S34), will induce the woven fabric of μ GTs (Fig. 4f–h, Supplementary Fig. S34).

The region-defined patterns of RGO network are also available through the powerful SARA-GO. As presented in Fig. 4i and Supplementary Fig. S35, by pressing a Cu grid (200 μm in side length) on Pt foil and exposing them to the GO suspension, we can achieve the RGO patterns on Pt foil after removing the Cu grid. The region-confined 3D graphene network remains well with freeze-drying (Fig. 4j). Depending on the Cu masks, a variety of specific patterns on nonconductive substrates can also be designed for various applications (Supplementary Fig. S36&37).

SARA-GO for construction of binder-free lithium-ion batteries (LIBs). Apart from the construction of unique graphene configurations of practical importance mentioned above, the SARA-GO method enabling the self-organization of 3D graphene network on various conductive substrates will largely facilitates the fabrication of graphene electrodes, and thus benefits the device applications.

As one of the important energy storage devices, rechargeable LIBs have drawn worldwide interest^{2,3}. However, graphite, the most commonly used commercial anode material, encounters serious disadvantages such as low theoretical specific capacity (372 mAh g^{-1}) and limited rate capability. As a result, great efforts are being devoted to developing new electrode materials for high performance LIBs. Graphene is expected to be a good candidate as a high-power and high-energy electrode material due to its intrinsically superior electrical conductivity, excellent mechanical flexibility, remarkable thermal conductivity, high surface area^{29,30}, and high chemical diffusivity of Li, $\sim 10^{-7}$ – 10^{-6} ($\text{cm}^2 \text{s}^{-1}$)^{31,32}. Herein, the SARA-GO method provides a straightforward route to assemble graphene network on the Cu foil in the form of 3D pore-interconnected structure, which can be directly used as anode electrode in LIBs without need of any

ancillary materials such as binders and conductive additives required for the conventional LIB fabrication.

The cropped Cu foil (Fig. 5a) was first deposited with RGO network on one side via SARA-GO (Fig. 5b). After slightly washing with aqueous HCl to remove the Cu oxides, the freeze-dried sample (Fig. 5c) as anode was directly assembled in a coin battery (Fig. 5d).

As shown in Fig. 5e, the RGO/Cu electrode shows typical cyclic voltammogram (CV) curves (1 to 5 cycles) of the carbonaceous anode materials at a scan rate of 0.5 (mV s^{-1}). The peak at around 0.8 V can be ascribed to the decomposition of the electrolyte on the surface of RGO, leading to the formation of the solid electrolyte interphase (SEI) layer^{33,34}. The CV curves of the second to the fifth cycle almost overlap, implying an excellent cycling ability of the RGO/Cu electrode.

Fig. 5f shows the galvanostatic charge/discharge profiles of the RGO/Cu electrode between 0.01–3 V at a current density of 0.1 A g^{-1} . The initial discharge and charge specific capacities are 2472 and 1605 mAh g^{-1} , respectively. The irreversible capacity loss is generally attributed to the formation of SEI^{33,34}. The RGO/Cu electrode becomes stable at the ninth cycle with a capacity of 1076 mAh g^{-1} , which is about 2.9 times higher than the theoretical one of graphite (372 mAh g^{-1}).

Fig. 5g shows the cycling performance and the corresponding coulombic efficiency at a current of 0.3 A g^{-1} after aging at 0.1 A g^{-1} for 10 cycles. The discharge capacity stabilizes at 725 mAh g^{-1} for 60 cycles, which is about 2 times higher than the theoretical capacity of graphite, superior to that of many other carbon materials (Table S3) including carbon nanosprings³⁵, carbon nanocages³⁶, carbon nanofibers (CNF)³⁷, carbon nanotubes (CNT)³⁸, CNF/CNT³⁹, N-doped graphene⁴⁰ and N,S-codoped porous graphene⁴¹, as well as metal oxides of CoMn_2O_4 microspheres⁴², and their composites such as MnO_2/CNT ⁴³ and $\text{Fe}_3\text{O}_4/\text{RGO}$ ⁴⁴. At the meanwhile, the coulombic efficiency of the battery retained at nearly 100% during the cycling, showing an excellent reversibility. Furthermore, the 3D RGO/Cu-based battery has also a great rate behavior as tested under variable rates from 0.1 A g^{-1} to 20 A g^{-1} (Fig. 5h). Even at 20 A g^{-1} , the reversible capacity is still 231 mAh g^{-1} , which is closed to the highly N-doped carbon materials with excellent performance^{34,45}. Remarkably, after the high-rate measurements, the specific capacities of the RGO/Cu electrode almost recover to the initial values cycled at 100 mA g^{-1} . A long-term cycling stability has also been carried out at a high current density of 2 A g^{-1} . As shown in Fig. 5i, the anode material shows stable cycling behavior, and the reversible capacity of up to about 500 mAh g^{-1} is achieved for 300 cycles, which is still ca. 134% of the theoretical capacity of graphite. On the other hand, the electrochemical impedance spectra of the RGO/Cu electrode before and after cycling at 0.3 A g^{-1} for 100 cycles indicate the activated and improved reaction kinetics upon cycling, and the good contact between the RGO/Cu electrode and the current collector (Supplementary Fig. S38).

Discussion

As we know, GO can be reduced by strong reduction reagents such as hydrazine⁸. However, GO as a strong oxidant is paid the little attention. In fact, GO has the capability to oxidize Fe^{2+} to Fe^{3+} in despite of the relatively high redox potential of +0.77 V (vs. standard hydrogen electrode, SHE) for ($\text{Fe}^{2+}/\text{Fe}^{3+}$)⁴⁶. Example also includes the oxidation of iodide ions (I^-) into neutral iodine (I_2) (+0.54 V vs. SHE for I^-/I_2) by GO suspension⁴⁷. Therefore, it is reasonable to observe that GO was reduced by active metals such as Al, Fe, Cu^{20–22}.

By curve fitting analysis of the XPS results (Fig. 2h), we can find that the hydroxyl, epoxy and carbonyl groups decrease drastically, while the carboxylic acid groups remain relatively stable. Considering that the epoxy and hydroxyl groups are the main active oxide groups of GO for the typical reduction process^{48,49}, and epoxy group can also convert to hydroxyl group in aqueous acidic solution, we

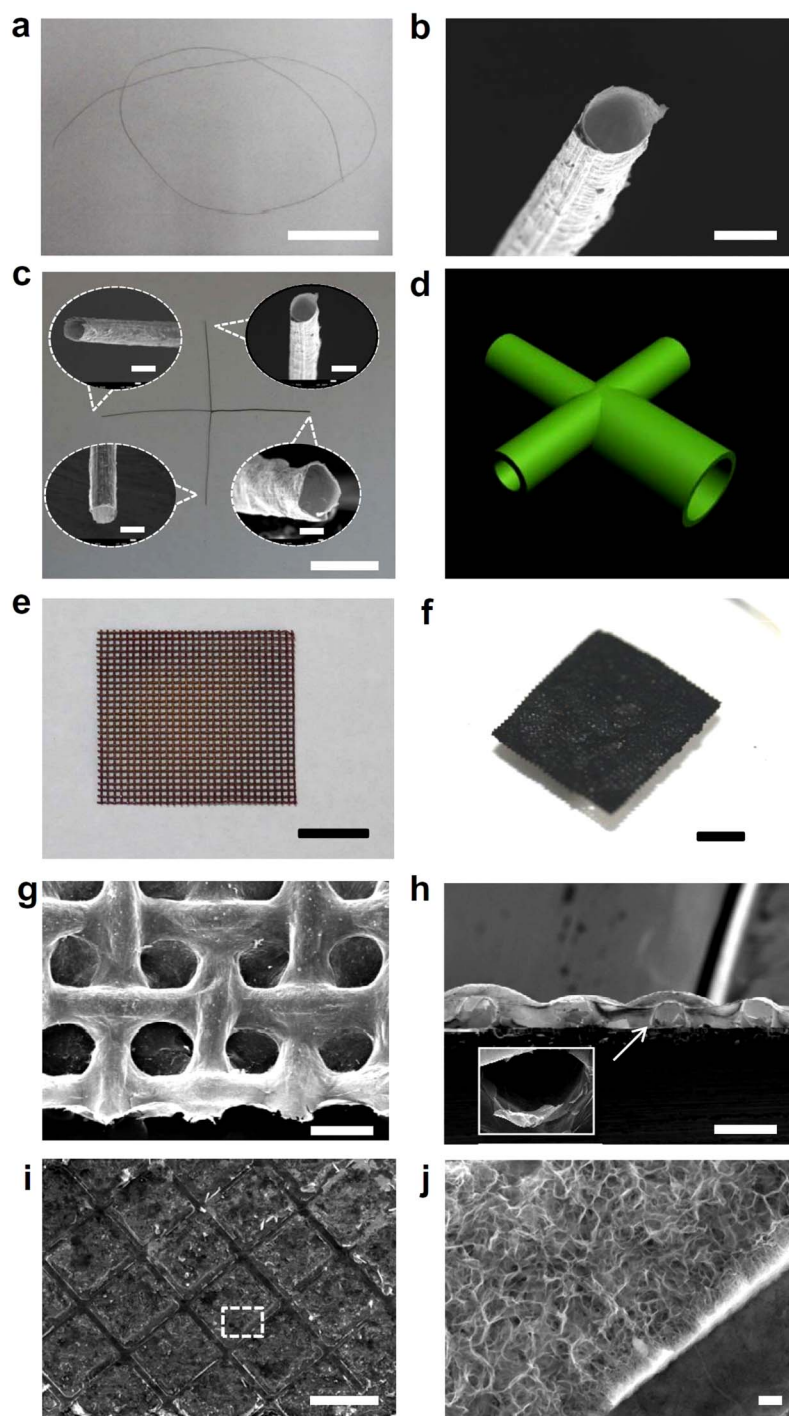


Figure 4 | Fabrication of graphene microtubes, four-way pipe, multi-channel network and graphene micropatterns via SARA-GO process. (a and b) Photograph and SEM image of the graphene microtube produced by SARA-GO on Cu wire. (c) Photograph of a four-way tube with the corresponding SEM images of the nozzles. (d) The corresponding schematic diagram of (c). (e and f) The Cu mesh and the derived graphene mesh by SARA-GO, respectively. (g and h) Top and side SEM images of graphene mesh in (f), respectively. (i) Graphene patterns on the Pt foil and (j) the enlarged view of the marked area in (i). Scale bars: (a, c, e, f), 1 cm; (b), 50 μm ; (g), (h), 500 μm ; (i), and (c) inset, 100 μm ; (j), 1 μm .

proposed the reaction mechanism via an electron transfer process of GO with hydroxyl groups as exemplified model in Figure 6. The hydrons are easy to form the complex with the oxygen-related groups in GO, which could induce a dehydration process and allow the positively charged GO system to receive the electrons from the active metals^{20–22}. Accordingly, metal ions produced by electron-lost metals could combine the hydroxide (OH^-) ions to balance hydrogen (H^+). These metastable metal hydroxides then further performed a

dehydration process to form metal oxides as we have experimentally observed the formation of such metal oxides as Cu_2O (Fig. 2c), ZnO (Supplementary Fig. S7–S9), and Fe_3O_4 (Supplementary Fig. S10&S11) during SARA-GO.

Besides, we also performed the first principle calculation to compare the electron properties of metal surfaces on the basis of the work functions. The work function is the minimum energy required to release electrons from the reactive surface, which should give some

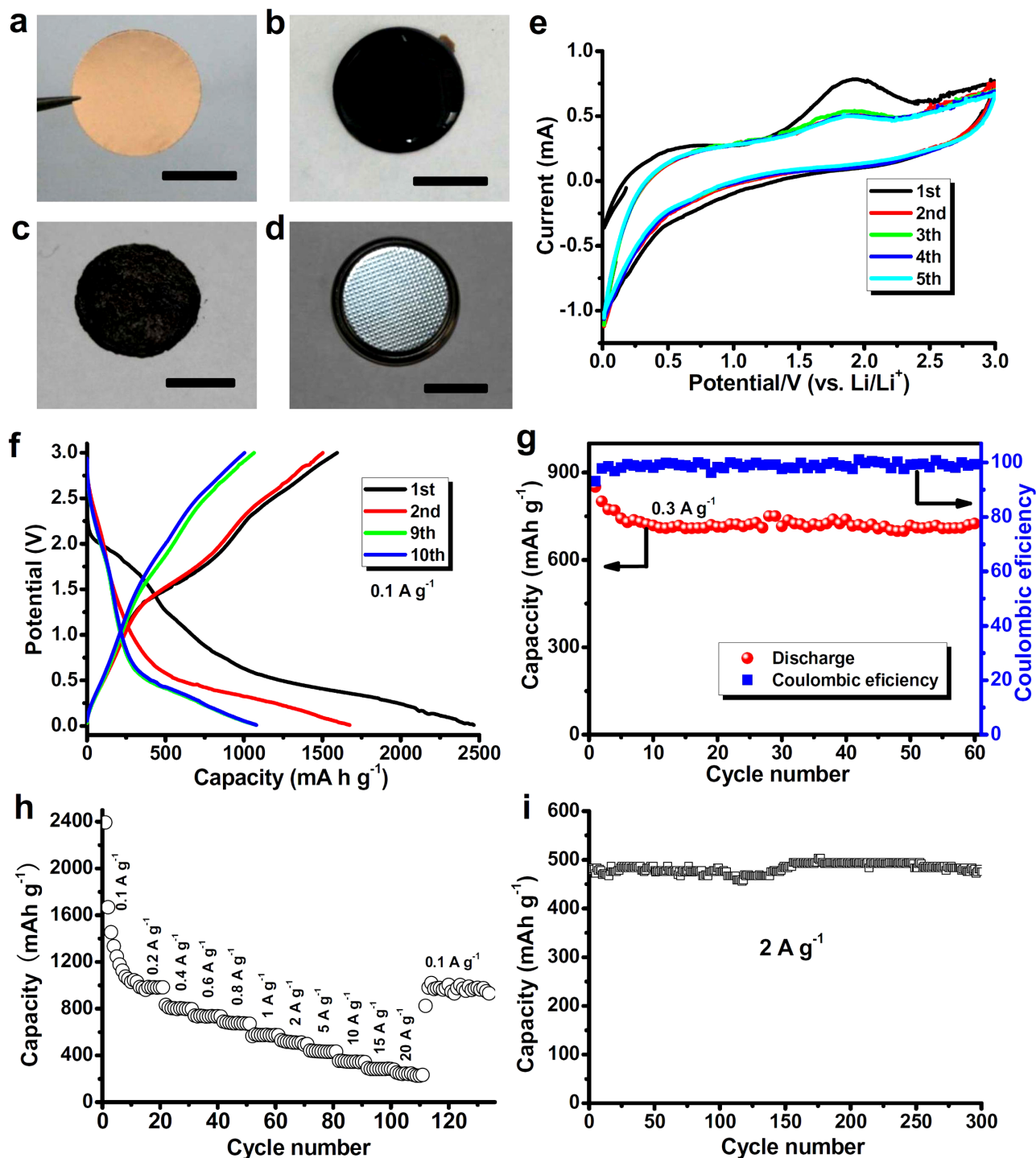


Figure 5 | Characterization of the binder-free LIBs. (a) Photograph of the trimmed Cu foil with circular shape. (b) RGO assembled on Cu foil by SARA-GO. (c) The 3D RGO formed on Cu foil after lyophilization process. (d) The Li coin battery using the Cu foil supported 3D RGO as anode. (e) CVs of the first five cycles of the RGO/Cu electrode. (f) Charge and discharge voltage profiles for the first, second, ninth, and tenth cycles between 0.01–3.00 V at a current density of 0.1 A g⁻¹. (g) Discharge capacity vs. cycle number of the coin battery at a current density of 0.3 A g⁻¹ and the corresponding coulombic efficiency. (h) Rate capability test at various current densities. (i) Cycling performance of the coin battery at a current density of 2 A g⁻¹ for 300 cycles. The scale bars in (a–d) are 1 cm.

clues why different metals have the quite different performances for reducing GO. In our calculation the generalized gradient approximation with the Perdew-Burke-Ernzerhof functional⁵⁰ was used, the basis set contains plane waves up to an energy cutoff of 380 eV and the structure is relaxed until the force on each atom is less than 0.03 eV/Å in the Vienna ab initio software package (VASP)^{51,52}.

We performed the calculation on several metal slabs of Zn (0001), Al (111), Cu(111), Pt (111) and Au (111) surfaces with seven layers as examples using Periodic Boundary Conditions (PBC) (Supplementary Fig. S39). The work functions of these metals are 4.02 eV, 4.13 eV, 4.73 eV, 5.85 eV and 5.01 eV, respectively. These results indicate the capacity to lose electrons of the different metals.

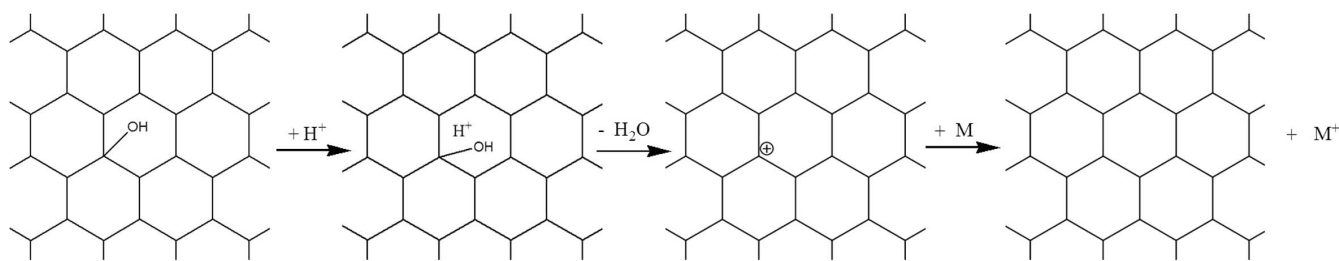


Figure 6 | The proposed reaction mechanism. The hydronium forms a complex with the oxide groups (e.g., hydroxyl group) in GO. After the dehydration process, the positively charged GO gets the electrons from the active metal (M) and the metal is oxidized to M^+ ions. Only one electron transfer is presented in this schematic diagram.

Obviously, the active metals like Zn, Al and Cu are much more active than Pt and Au for GO reduction in consistent with the experimental observation. Although the difficulty to directly reduce GO on inert metals of Pt and Au, the SARA-GO (Figure 1b) developed in this study provide the solution.

It is also notable that the SARA-GO method will generate the graphene assemblies with easy in-situ functionalization. As can be seen in Fig. 2c and Supplementary Fig. S7–S11, the functional components such as Cu_2O , ZnO and Fe_3O_4 , if not washed away by aqueous HCl, could be spontaneously attached on the graphene sheets during the SARA-GO process. Therefore, new functions could be expected due to these incorporated components. As an example shown in Supplementary Fig. S40, the as-prepared ZnO-containing graphene film presents the fast photocurrent response with good repeatability upon exposure to a daylight lamp (100 W).

In conclusion, a general method of substrate-assisted reduction and assembly of graphene oxide has been developed for spontaneous deposition of 3D graphene network on arbitrary conductive substrates without any additional reducing agent. The SARA-GO process offers a facile, but efficient approach for constructing a variety of unique graphene assemblies of practical importance. For examples, graphene microtubes, four-way pipes, spiral tubes, multi-channel networks, and micropatterns have been conveniently manufactured by using Cu or Fe wires and meshes as templates. The SARA-GO enabling the self-organization of 3D graphene network on various conductive substrates largely facilitates the fabrication of graphene electrodes. The binder-free LIBs using spontaneously deposited 3D graphene network on Cu foil as anode materials have been demonstrated, which exhibit high capacity, cycling stability and rate performance superior to many other carbon-based materials and metal oxide composites. The versatile SARA-GO method with significantly improved processability of graphenes will benefit a variety of applications beyond those specifically demonstrated in this preliminary study.

Methods

Synthesis of Graphene Oxide (GO). GO was prepared from natural graphite powder via acid-oxidation according to a modified Hummers method as mentioned in our previous papers^{53,54}.

Spontaneous deposition of 3D RGO network on Al, Zn, Fe, Co, Cu foils. Zn, Fe, Cu, Co and Al foils were exposure to 1 mg/mL GO solution for a certain time (e.g., 1–12 h) at ambient condition (Supplementary Fig. S1), and RGO was spontaneously assembled on the metal foils. The metal oxides on RGO were carefully washed away with over 2 M HCl aqueous solution, followed with deionized water. The lyophilization was carried out to get the 3D RGO network. All the metal foils were purchased from Alfa Aesar with a purity of >99.9%. To accelerate the reaction and prevent the passivation effect due to the coating of the produced nonconductive metal oxides, a mild temperature of 60 °C is also applied on demand.

Spontaneous deposition of RGO network on the surfaces of inert metals of Au, Ag, Pt and semiconducting Si (N-type). We first deposited a layer of Cu on one sides of Au, Ag, Pt foils, and Si wafer by vacuum sputtering, which were then exposure to 1 mg/mL GO solution for several hours. Apart from the Cu sides, RGO network was also spontaneously deposited on the Cu-free sides of Au, Ag, Pt foils and Si wafer. The alternative method for depositing RGO network on the surface of inert metals and Si

is covering them by Cu foil partly, followed by directly immersing them in 1 mg/mL GO solution for a certain time.

Spontaneous deposition of RGO network on the surfaces of Au, Ag, Pt nanostructures.

The preparation of Au, Ag, Pt nanostructures with different size shape on Cu foils were carried out as described in our previous publications^{26,55}. Briefly, on sides of the Cu foils were contacted with aqueous 0.01 M H_2PtCl_6 , 0.02 M $AgNO_3$, and 0.01 M H_2PtCl_6 solutions for 1 min, respectively, for the deposition of the nanostructured Au, Ag or Pt with different sizes and shapes on Cu foils as shown in Supplementary Fig. S19–S22. Subsequently, Cu foils were washed with HCl solution and deionized water several times carefully before further experiments. For the formation of RGO network on the nanostructures, the Cu foils with nanostructured Au, Ag, Pt were exposed to 1 mg/mL GO solution for 8 h, which were then washed by HCl solution, deionized water several times, characterized after lyophilization.

Spontaneous deposition of RGO network on indium-tin oxide (ITO) surface. ITO glass was half covered with Cu layer by vacuum sputtering, which was then exposed to 1 mg/mL GO solution for 12 h at room temperature (Supplementary Fig. S25). After that, the ITO was washed with deionized water slightly before lyophilization. Finally, the remained Cu was removed from the ITO glass carefully, and the region of RGO on ITO was still transparent due to the short reaction time.

Spontaneous deposition of RGO network on carbon film. We used the carbon film coated Cu-based TEM grid as an example to demonstrate the effective deposition of RGO on carbon film. A carbon-coated Cu TEM grid was immersed in the 1 mg/mL GO solution for 10 h, which was then washed with aqueous HCl and deionized water, followed by lyophilization before characterization.

Spontaneous deposition of RGO network on graphene film. A two step deposition of RGO was devised for this purpose (Supplementary Fig. S27&28). The graphene film supported by Cu was first prepared by exposure of Cu foil to the 0.5 mg/mL GO solution for 10 h, which was washed with HCl solution and deionized water several times carefully, followed by naturally drying to form a graphene film on Cu. This Cu supported graphene film was then immersed in 1 mg/mL GO solution for 10 h for the further deposition of RGO on the preformed graphene film. The RGO on graphene film could be directly peeled off from the Cu foil or separated from the Cu foil by 1 M $FeCl_3$ treatment for 0.5 h. Finally, the 3D RGO assembled on graphene film was collected after washing with deionized water and lyophilization.

Preparation of graphene microtubes (μ GTs). The formation of μ GTs is schematically shown in Supplementary Fig. S29. A Cu wire was immersing into 1 mg/mL GO solution for 10 h to allow the assembly of RGO along the Cu wire. Then the wet graphene wrapped Cu wire was taken out from the solution, and densely packed graphene layer surrounding Cu wire was formed after drying naturally. Subsequently, μ GTs with a diameter depending on the supporting Cu wire were collected after etching Cu wire in an aqueous 2.5 M $FeCl_3$ solution containing 0.5 M HCl and thoroughly washing with distilled water. The Cu wire can not only reduce the GO to RGO, but also act as the support during the drying process. The μ GTs with diameters of ca. 100 (Supplementary Fig. S30) and 40 μ m (Fig. 4b) were produced by choosing the Cu wires with corresponding diameters as supporting core.

The preparation of Y-shaped μ GT with spiral structure, four-way pipe and multi-channel network of graphenes. Based on the formation of μ GTs mentioned above, different configurations of Cu wires (Supplementary Fig. S32&33), and Cu or Fe meshes (Supplementary Fig. S34) were exposed to the 1 mg/mL GO solution to allow the formation of Y-shaped μ GT with spiral structure, four-way pipe and multi-channel network of graphenes.

The preparation of RGO pattern on Pt foil. As presented in Supplementary Fig. S35, by pressing a Cu grid (200 μ m in side length) on Pt foil and then exposing them to the 1 mg/mL GO suspension for 12 h, we can achieve the RGO patterns on Pt foil after removing the Cu grid. The region-confined 3D graphene network remains well with freeze-drying (Fig. 4i&j).



The preparation of region-defined pattern of RGO on SiO₂. Cu islands on SiO₂ were first obtained by vacuum sputtering with a Cu grid (400 μm in side length) as mask (Supplementary Fig. S36), which was then immersed in 1 mg/mL GO for 12 h to assemble the RGO on the Cu deposited regions. 3D porous RGO patterns on SiO₂ were produced by freeze-drying procedure. The patterns of RGO film were obtained with naturally drying.

Fabrication of 3D RGO/Cu electrode. Firstly, the trimmed Cu foil with circular shape was immersed in 1 mg/mL GO solution for 10 h for the spontaneous assembly of RGO on Cu foil. After slightly washing with aqueous HCl, the sample was freeze-dried to keep 3D pore-interconnected graphene structure on Cu, which was directly used as working electrode in LIBs without need of any ancillary materials such as binders and conductive additives required for the conventional LIB fabrication.

LIB investigation. The as-obtained sample was directly used as working electrode without any ancillary materials for cell assembly. A lithium foil was used as the counter electrode and a solution of 1 M LiPF₆ in ethylene carbonate (EC)/dimethyl carbonate (DMC)/diethyl carbonate (DEC) (1 : 1 : 1 in volume) was used as electrolyte. The assembly of the cells was performed in an argon-filled glove box. The cells were then aged for 8 h before measurement. The cycling tests were charged and discharged using an LAND CT2001A test station. The impedance spectra were obtained by applying a sine wave with amplitude of 5 mV over the frequency range from 100 kHz to 0.01 Hz. The weights of graphenes on Cu foil were determined by measuring more than 10 parallel samples under the same condition. A mean value was used in this study.

Characterization. The morphology of the samples was determined by FET TECNAI F30 high resolution transmission electron microscopy (HR-TEM) at an acceleration voltage of 200 kV. Field-emission scanning electron microscope (FE-SEM) images and EDS data of the samples were taken on JSM-7001F SEM unit. X-ray diffraction (XRD) patterns were obtained by using a Netherlands 1,710 diffractometer with a Cu K α irradiation source ($\lambda = 1.54 \text{ \AA}$), and a self-calibration process was performed with a SiO₂ internal standard sample prior to target measurement. X-ray Photoelectron spectroscopy (XPS) data were obtained with an ESCALab220i-XL electron spectrometer from VG Scientific using 300 W AlK α radiation. The base pressure was about 3×10^{-9} mbar. The binding energies were referenced to the C 1 s line at 284.8 eV from adventitious carbon.

- Sun, Y. Q., Wu, Q. & Shi, G. Q. Graphene based new energy materials. *Energy Environ. Sci.* **4**, 1113–1132 (2011).
- Huang, X., Qi, X. Y., Boey, F. & Zhang, H. Graphene-based composites. *Chem. Soc. Rev.* **41**, 666–686 (2012).
- Chen, D., Tang, L. H. & Li, J. H. Graphene-based materials in electrochemistry. *Chem. Soc. Rev.* **39**, 3157–3180 (2010).
- Shao, Y. Y. *et al.* Graphene based electrochemical sensors and biosensors: a review. *Electroanal.* **22**, 1027–1036 (2010).
- Chen, H., Muller, M. B., Gilmore, K. J., Wallace, G. G. & Li, D. Mechanical strong, electrically conductive, and biocompatible graphene paper. *Adv. Mater.* **20**, 3557–3561 (2008).
- Schwierz, F. Graphene transistors. *Nat. Nanotechnol.* **5**, 487–496 (2010).
- Park, S. J. & Ruoff, R. S. Chemical methods for the production of graphenes. *Nat. Nanotechnol.* **4**, 217–224 (2009).
- Stankovich, S. *et al.* Synthesis of graphene-based nanosheets via chemical reduction of exfoliated graphite oxide. *Carbon* **45**, 1558–1565 (2007).
- Su, C. Y. *et al.* Highly efficient restoration of graphitic structure in graphene oxide using alcohol vapors. *ACS Nano* **4**, 5285–5292 (2010).
- Fan, X. B. *et al.* Deoxygenation of exfoliated graphite oxide under alkaline conditions: a green route to graphene preparation. *Adv. Mater.* **20**, 4490–4493 (2008).
- Park, S. *et al.* Aqueous suspension and characterization of chemically modified graphene sheets. *Chem. Mater.* **20**, 6592–6594 (2008).
- Gao, W., Alemany, L. B., Ci, L. J. & Ajayan, P. M. New insights into the structure and reduction of graphite oxide. *Nat. Chem.* **1**, 403–408 (2009).
- Moon, I. K., Lee, J., Ruoff, R. S. & Lee, H. Reduced graphene oxide by chemical graphitization. *Nat. Commun.* **1**, 1 (2010).
- Feng, H. B., Cheng, R., Zhao, X., Duan, X. F. & Li, J. H. A low-temperature method to produce highly reduced graphene oxide. *Nat. Commun.* **4**, 1539 (2013).
- Mao, S., Pu, H. H. & Chen, J. H. Graphene oxide and its reduction: modeling and experimental progress. *RSC Adv.* **2**, 2643–2662 (2012).
- Hu, C. G. *et al.* Newly-designed complex ternary Pt/PdCu nanoboxes anchored on three-dimensional graphene framework for highly efficient ethanol oxidation. *Adv. Mater.* **24**, 5493–5498 (2012).
- Wu, Z. S. *et al.* Three-dimensional graphene-based macro- and mesoporous frameworks for high-performance electrochemical capacitive energy storage. *J. Am. Chem. Soc.* **134**, 19532–19535 (2012).
- Zhao, Y. *et al.* A versatile, ultralight, nitrogen-doped graphene framework. *Angew. Chem. Int. Ed.* **51**, 11371–11375 (2012).
- Xu, Y. X., Sheng, K. X., Li, C. & Shi, G. Q. Self-assembled graphene hydrogel via a one-step hydrothermal process. *ACS Nano* **4**, 4324–4330 (2010).
- Fan, Z. J. *et al.* Facile synthesis of graphene nanosheets via Fe reduction of exfoliated graphite oxide. *ACS Nano* **5**, 191–198 (2011).
- Fan, Z. J. *et al.* An environmentally friendly and efficient route for the reduction of graphene oxide by aluminum powder. *Carbon* **48**, 1670–1692 (2010).
- Cao, X. B. *et al.* Ambient fabrication of large-area graphene films via a synchronous reduction and assembly strategy. *Adv. Mater.* (2013), DOI: 10.1002/adma.201300586.
- Yin, M. *et al.* Copper oxide nanocrystals. *J. Am. Chem. Soc.* **127**, 9506–9511 (2005).
- Borghain, K., Murase, N. & Mahamuni, S. Synthesis and properties of Cu₂O quantum particles. *J. Appl. Phys.* **92**, 1292–1297 (2002).
- Li, Y. R., Sheng, K. X., Yuan, W. J. & Shi, G. Q. A high-performance flexible fibre-shaped electrochemical capacitor based on electrochemically reduced graphene oxide. *Chem. Commun.* **49**, 291–293 (2013).
- Qu, L. T. & Dai, L. M. Substrate-enhanced electroless deposition of metal nanoparticles on carbon nanotubes. *J. Am. Chem. Soc.* **127**, 10806–10807 (2005).
- Hu, C. G. *et al.* Graphene microtubules: controlled fabrication and site-specific functionalization. *Nano Lett.* **12**, 5879–5884 (2012).
- Zhao, Y. *et al.* Large-scale spinning assembly of neat, morphology-defined, graphene-based hollow fibers. *ACS Nano* **7**, 2406–2412 (2013).
- Novoselov, K. S. *et al.* Electric field effect in atomically thin carbon films. *Science* **306**, 666–669 (2004).
- Geim, A. K. Graphene: status and prospects. *Science* **324**, 1530–1534 (2009).
- Persson, K. *et al.* Lithium diffusion in graphitic carbon. *J. Phys. Chem. Lett.* **1**, 1176–1180 (2010).
- Uthaisar, C. & Barone, V. Edge effects on the characteristics of Li diffusion in graphene. *Nano Lett.* **10**, 2838–2842 (2010).
- Hu, Y. S. *et al.* Synthesis of hierarchically porous carbon monoliths with highly ordered microstructure and their application in rechargeable lithium batteries with high-rate capability. *Adv. Funct. Mater.* **17**, 1873–1878 (2007).
- Qie, L. *et al.* Nitrogen-doped porous carbon nanofiber webs as anodes for lithium ion batteries with a superhigh capacity and rate capability. *Adv. Mater.* **24**, 2047–2050 (2012).
- Wu, X., Liu, Q., Guo, Y. & Song, W. Superior storage performance of carbon nanosprings as anode materials for lithium-ion batteries. *Electrochem. Commun.* **11**, 1468–1471 (2009).
- Li, G. D., Xu, L. Q., Hao, Q., Wang, M. & Qian, Y. T. Synthesis, characterization and application of carbon nanocages as anode materials for high-performance lithium-ion batteries. *RSC Adv.* **2**, 284–291 (2012).
- Habazaki, H., Kiri, M. & Konno, H. High rate capability of carbon nanofilaments with platelet structure as anode materials for lithium ion batteries. *Electrochem. Commun.* **8**, 1275–1279 (2006).
- Shen, J. M. & Feng, Y. T. Formation of flower-like carbon nanosheet aggregations and their electrochemical application. *J. Phys. Chem. C* **112**, 13114–13120 (2008).
- Zhang, J. *et al.* CNFs@CNTs: superior carbon for electrochemical energy storage. *Adv. Mater.* **20**, 1450–1455 (2008).
- Wu, Z. S., Ren, W. C., Xu, L., Li, F. & Cheng, H. M. Doped graphene sheets as anode materials with superhigh rate and large capacity for lithium ion batteries. *ACS Nano* **7**, 5463–5471 (2011).
- Wang, Z. L., Xu, D., Wang, H. G., Wu, Z. & Zhang, X. B. In situ fabrication of porous graphene electrodes for high-performance energy storage. *ACS Nano* **7**, 2422–2430 (2013).
- Hu, L. *et al.* CoMn₂O₄ spinel hierarchical microspheres assembled with porous nanosheets as stable anodes for lithium-ion batteries. *Sci. Rep.* **2**, 986–993 (2012).
- Reddy, A. L. M., Shaijumon, M. M., Gowda, S. R. & Ajayan, P. M. Coaxial MnO₂/carbon nanotube array electrodes for high-performance lithium batteries. *Nano Lett.* **9**, 1002–1006 (2009).
- Wei, W. *et al.* 3D graphene foams cross-linked with pre-encapsulated Fe₃O₄ nanospheres for enhanced lithium storage. *Adv. Mater.* (2013), DOI: 10.1002/adma.201300445.
- Hu, C. G. *et al.* Highly nitrogen-doped carbon capsules: scalable preparation and high-performance applications in fuel cells and lithium ion batteries. *Nanoscale* **5**, 2726–2733 (2013).
- Xue, Y. H. *et al.* Oxidizing metal ions with graphene oxide: the *in situ* formation of magnetic nanoparticles on self-reduced graphene sheets for multifunctional applications. *Chem. Commun.* **47**, 11689–11691 (2011).
- Pei, S. F., Zhao, J. P., Du, J. H., Ren, W. C. & Cheng, H. M. Direct reduction of graphene oxide films into highly conductive and flexible graphene films by hydrohalic acids. *Carbon* **48**, 4466–4474 (2010).
- Liu, L. *et al.* Amorphous structural models for graphene oxides. *Carbon* **50**, 1690–1698 (2012).
- Dreyer, D. R., Park, S. J., Bielawski, C. W. & Ruoff, R. S. The chemistry of graphene oxide. *Chem. Soc. Rev.* **39**, 228–240 (2010).
- Perdew, J. P., Burke, K. & Ernzerhof, M. Generalized gradient approximation made simple. *Phys. Rev. Lett.* **77**, 3865–3868 (1996).
- Kresse, G. & Furthmüller, J. Efficient iterative schemes for ab initio total-energy calculations using a plane-wave basis set. *Phys. Rev. B* **54**, 11169–11186 (1996).
- Kresse, G. & Furthmüller, J. Efficiency of ab-initio total energy calculations for metals and semiconductors using a plane-wave basis set. *Comput. Mat. Sci.* **6**–15 (1996).
- Li, Y. *et al.* An electrochemical avenue to green-luminescent graphene quantum dots as potential plectron-acceptors for photovoltaics. *Adv. Mater.* **23**, 776–780 (2011).



54. Li, Y. *et al.* Nitrogen-doped graphene quantum dots with oxygen-rich functional groups. *J. Am. Chem. Soc.* **134**, 15–18 (2012).
55. Qu, L. T., Dai, L. M. & Osawa, E. Shape/size-controlled syntheses of metal nanoparticles for site-selective modification of carbon nanotubes. *J. Am. Chem. Soc.* **128**, 5523–5532 (2006).

Acknowledgements

This work is sponsored by National Basic Research Program of China (2011CB013000), NSFC (No. 21004006, 21174019, 51161120361), Fok Ying Tong Education Foundation (No. 131043), the 111 Project B07012, and research foundation for the doctoral program of higher education of China (20101101120036).

Author contributions

L.Q. conceived and designed the experiments. C.H., X.Z. and Y.Z. prepared the samples and performed characterization. L.L. performed the computer calculation. L.Q. discussed with

L.J. for the experimental design and results. L.Q., C.H. and L.L. were mainly responsible for preparing the manuscript with further inputs from other authors. All the authors discussed the results and commented on the manuscript.

Additional information

Supplementary information accompanies this paper at <http://www.nature.com/scientificreports>

Competing financial interests: The authors declare no competing financial interests.

How to cite this article: Hu, C.G. *et al.* Spontaneous Reduction and Assembly of Graphene oxide into Three-Dimensional Graphene Network on Arbitrary Conductive Substrates. *Sci. Rep.* **3**, 2065; DOI:10.1038/srep02065 (2013).



This work is licensed under a Creative Commons Attribution-NonCommercial-NoDerivs 3.0 Unported license. To view a copy of this license, visit <http://creativecommons.org/licenses/by-nc-nd/3.0>